한국공작기계학회논문집 Vol.17 No.2 2008. 4.
Transactions of the Korean Society of Machine Tool Engineers

3-DOF Parallel Micromanipulator : Design Consideration

Jeongick Lee*, Dongchan Lee+, Changsoo Han++

(논문접수일 2007. 7. 27, 심사완료일 2007. 12. 3)

3차원 평형 마이크로조정장치 : 설계 고려사항

이정익*, 이동찬+, 한창수++

Abstract

For the accuracy correction of the micro-positioning industrial robot, micro-manipulator has been devised. The compliant mechanisms using piezoelectric actuators is necessary geometrically and structurally to be developed by the optimization approaches. The overall geometric advantage as the mechanical efficiencies of the mechanism are considered as objective functions, which respectively are the ratio of output displacement to input force, and their constraints are the vertical motion of supporting leg and the structural strength of manipulation. In optimizing the compliant mechanical amplifier, the sequential linear programming and an optimality criteria method are used for the geometrical dimensions of compliant bridges and flexure hinges. This paper presents the integrated design process which not only can maximize the mechanism feasibilities but also can ensure the positioning accuracy and sufficient workspace. Experiment and simulation are presented for validating the design process through the comparisons of the kinematical and structural performances.

Key Words : IC Micromanipulator(IC 마이크로 조정장치), Kinematics and Compliance(기구학과 컴플라이언스), Compliant Mechanical Amplifier(컴플리언트 증폭기), Compliant Bridge(컴플리언트 브릿지), Flexure Hinge(플랙셔 힌지), Shape Optimization(형상 최적화)

* 인하공업전문대학 기계시스템공학부 기계설계과 (jilee@inhatc.ac.kr)
주소: 402-752 인천광역시 남구 용현동 253번지
+ 한양대학교 기계공학과 대학원
++ 한양대학교 기계공학과

Notation

$\{\dot{\varphi}\}$	input velocity vector of serial chains
$\{\dot{u}\}$	output velocity of system
$[G_{\varphi}^{u}]$	Jacobian matrix
$[H_{\varphi\varphi}^{u}]$	Hessian matrix
$[{}_{i}K_{\varphi\varphi}]$	stiffness matrix for i-th ternary leg
σ_{ij}	stress tensor
ε_{ij}	strain tensor
x_i	design variable

1. Introduction

Recently, micro-mechanisms have been applied to such various fields as micro-machines, micro-surgery, bio-cells and so on. In order to apply micro-mechanisms to these fields, functionality of multi degree-of-freedom is essential to accurate micro positioning. For the high precision, flexure hinge has been commonly used as a substitute for mechanical joints. This configuration can minimize the additional backlash or inaccuracy caused through connection among modules. And in the view of the prevention of the positioning accuracy, a micro-positioning mechanism needs to be designed with the intention accurate flexure hinge modeling. The simulation based on FEM can be used and many researches have been performed[1~3]. In micro-structure design, in order to determine the feasible structural configuration with a flexural hinge under ultimate load, analyses must be incorporated for the differential stiffness originated from both geometry and the material's properties. The differential stiffness not only arises from such nonlinear stress-strain relationship as nonlinear elasticity but also a consequence of the configuration changes during the loading process due to the geometric dimensions. Many structural optimization designs are assumed to undergo small displacements relative to the configuration dimensions without differential stiffness. The structural topology is based on the linear relationship between force and structural stiffness. This assumption is applicable to a large class of problems. However, it is not valid for the case of a compliant mechanical design with the stiffness differential nonlinearities relative to the structural dimensions. To obtain the micro-structures with consideration of differential stiffness, it is necessary to consider the optimization design on the basis of nonlinear finite element analysis. These problems can be solved by using the fundamental structural optimization techniques based on the nonlinear finite element analysis. Structural optimization has become an integral part of the product design process. A considerable amount of micro-structural designs require the development of configuration design that fulfills various performance requirements such as stress, stiffness, and deflection[4~8].

Fig. 3 also shows the flexure representation of micro-manipulator. Fig. 1 shows the exact situation of micro amplifier mechanism(Fig. 6).

This paper presents the process of integrated design method which not only minimizes the infeasibilities of mechanism but also ensures positioning accuracy and sufficient workspace. This paper progresses as follows. System configuration of flexure hinge mechanism is defined by topology optimization and the detailed geometries are determined by shape and configuration optimization based on the gradient based optimization[9~11]. 3 D.O.F. micro-manipulator model is simulated.

2. Theoretical Considerations

As noted above, local compliances called to flexure hinge are divided into two categories: those chosen to satisfy connectivity requirements and those which, in addition, may have a significant influence on synthesis results. The division between categories is based on an inspection and, if necessary, a static test of the region around the attachment point. If the finite element model gives a reasonably accurate representation of the load-deflection behavior at the attachment point, then, a local compliance spring is chosen to satisfy substructure connectivity requirements. The spring stiffness must be feasibly compared with the stiffness of the adjoining structure but

not so large as to produce mathematical ill-conditioning of the synthesis stiffness, with consideration of structural constraints. Also, a careful evaluation of the local compliance is needed to avoid accuracy loss in the synthesis. After comparing static test and analysis results for a model of the local structure, a compliance structure is determined to compensate for any lack of detail in the finite element substructure model. This method can be replaced by a predictive approach based on increasing the modeling detail in those regions where local compliances have been identified to provide an analytical compliance value. In this point, the uncertainties concerning a structural synthesis must be included in the analysis.

These flexure hinges can easily be compensated for the limits of mechanically jointed robots, which have speed error, positioning errors, inertia effects, static friction and backlash in the mechanical joint in a relatively large workspace. This paper intends to present the integrated design process in the concept development of compliant mechanical amplifier of micro-manipulator. Fig. 1 shows a schematic configuration of 3 dimensional manipulator.

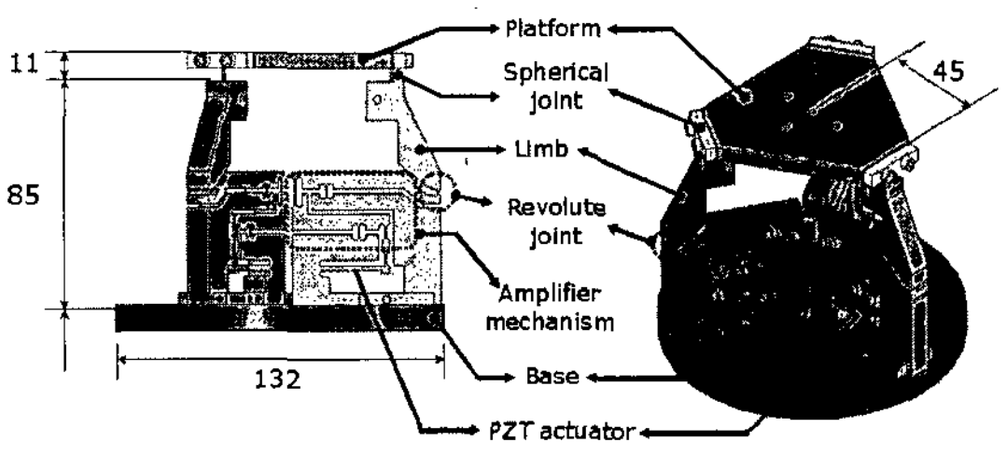

Fig. 1 Schematic configuration of manipulator[1]

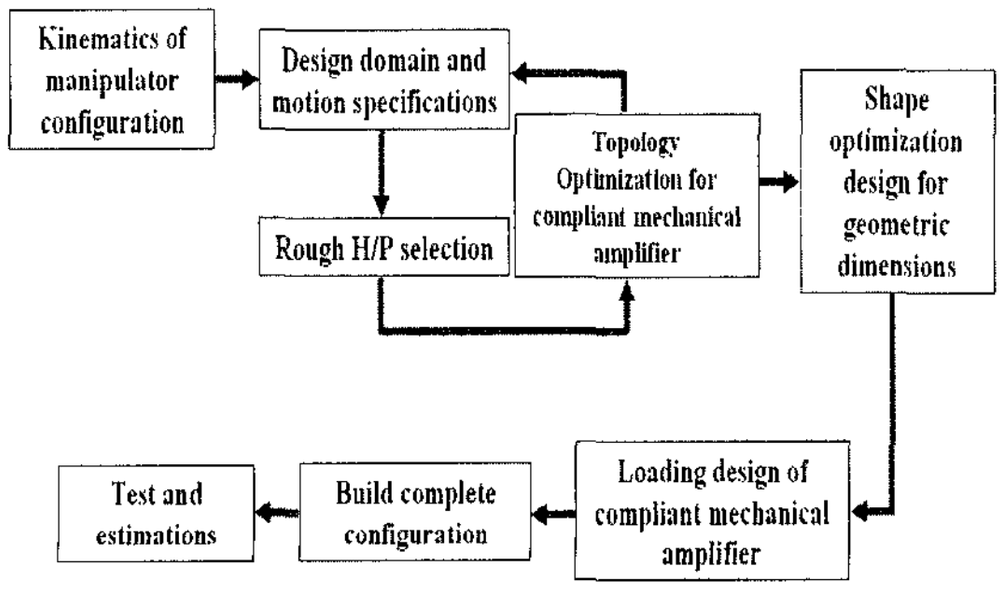

Fig. 2 Overall process for design of micro-manipulator

The overall process is shown in Fig. 2. Each stage is under the design specifications.

The detailed design specifications of a micro- manipulator are defined for a micro-manipulator as follows;

- Workspace: vertical motion, motion range(±100㎛, ± 0.1 deg), no backlash, minimal friction
- Structural specifications: bandwidth greater than 50 Hz, payload capacity, strength, linearity, repeatability
- Manufacturability: compactness, reliability, maintainability

2.1 Kinematics and Compliance Configuration Modeling

The configuration concept[1] is a parallel type mechanism composed of six serial chains shown in Fig. 3. Each chain consists of two spherical joints, revolute joint driving rotary input, base flexural joint, ternary base leg and supporting leg. The flexural hinges at base flexural joint and ternary base leg behave like mechanical joints by their compliances. These formulations use the generalized coordinate transformation. First-order kinematics relates the output velocity vector to the independent joint velocity vector. Using the chain rule, the first order time derivative of $\{u\}$ is

$$\{\dot{u}\} = \left(\partial\{u\}/\partial\{\varphi\}\right)\partial\{\varphi\}/\partial t = \left(\partial\{u\}/\partial\{\varphi\}\right)\{\dot{\varphi}\} = \left[G_{\varphi}^{u}\right]\{\dot{\varphi}\} \quad (1)$$

$$\{\ddot{u}\} = d\left[G_{\varphi}^{u}\right]\{\dot{\varphi}\}/dt = \left[G_{\varphi}^{u}\right]\{\ddot{\varphi}\} + \{\dot{\varphi}\}\left[H_{\varphi\varphi}^{u}\right]\{\dot{\varphi}\} \quad (2)$$

where, $\{\dot{u}\}$ and $\{\dot{\varphi}\}$ are the output velocity vector of system and the input velocity vaector of serial chains. $\left[G_{\varphi}^{u}\right]$ denotes the Jacobian matrix and $\left[G_{\varphi}^{u}\right] = \partial\{u\}/\partial\{\varphi\}$. $\left[H_{\varphi\varphi}^{u}\right]$ denotes Hessian matrix and $\left[H_{\varphi\varphi}^{u}\right] = \left(\partial\left[G_{\varphi}^{u}\right]/\partial\{\varphi\}\right) = \left(\frac{\partial}{\partial\{\varphi\}}\frac{\partial\{u\}}{\partial\{\varphi\}}\right)$.

In Fig. 3, the upper flexure hinges of support legs have only the rotational displacement. The flexure hinges at the joints can be considered as rotational springs and require force or moment to bend or expand or compress themselves. Each prismatic joint is the vertical motion of each compliant amplifier. Let the stiffness matrix for the i-th support leg with two flexure hinges can be written as,

$$\left[{}_iK_{\varphi\varphi}\right]=diag\left[{}_ik_1\ {}_ik_2\right] \tag{3}$$

where ${}_ik_j$ denotes the stiffness element of j-th flexural joint of i-th support leg. Then, in an equilibrium state, the potential energy in the mechanism can be defined as,

$$P.E.=\frac{1}{2}\sum_{i=1}^{n}d\{\varphi_i\}^T\left[{}_iK_{\varphi\varphi}\right]d\{\varphi_i\}$$

$$=\frac{1}{2}\left(\sum_{i=1}^{n}d\{u_i\}^T\left[{}_iG_u^{\varphi}\right]^T\left[{}_iK_{\varphi\varphi}\right]\left[{}_iG_u^{\varphi}\right]d\{u_i\}\right) \tag{4}$$

where, $\left[{}_iG_u^{\varphi}\right]$denotes the inverse Jacobian related to the infinitesimal displacement of $\{\varphi_i\}$ to that of $\{u_i\}$ and obtained by inversing of $\left[{}_iG_{\varphi}^{u}\right]$.

$\sum_{i=1}^{n}\left[{}_iG_u^{\varphi}\right]^T\left[{}_iK_{\varphi\varphi}\right]\left[{}_iG_u^{\varphi}\right]$ is the output stiffness matrix and a diagonal in the symmetric configuration and the effective output force due to $\delta\{u\}$ can be defined by the output stiffness matrix.

$$\delta\{T\}=\sum_{i=1}^{n}\left[{}_iG_u^{\varphi}\right]^T\left[{}_iK_{\varphi\varphi}\right]\left[{}_iG_u^{\varphi}\right]\delta\{u\} \tag{5}$$

The feasible configurations of compliant mechanism can found through topology and shape optimization designs.

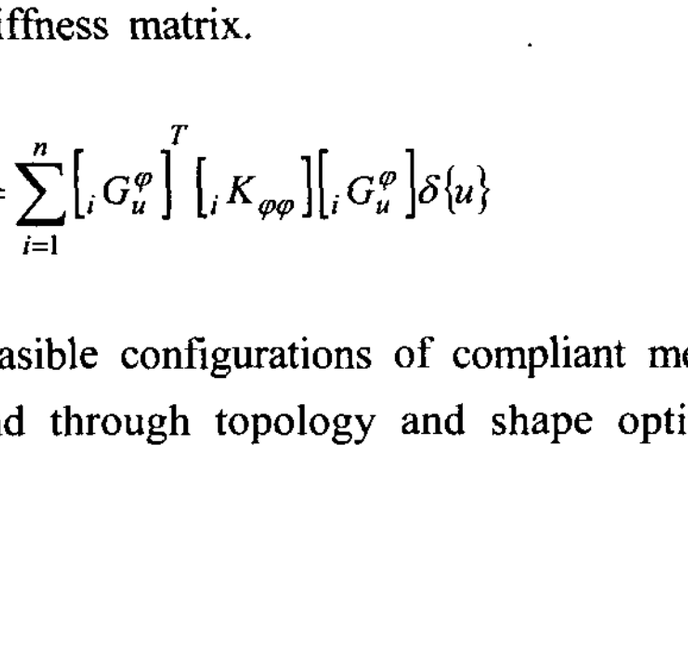

Fig. 3 Representation of micro-manipulator

2.2 Loading Condition of PZT-driven Compliant Mechanical Amplifier

The tension and compression of PZT bring about bending moment of compliant bridge shown in Fig. 4. For the feasible strength, the stresses in the compliant bridge and flexure hinges are limited to the effective stress that is 0.3 times yielding stress of material. Thus, the locations of PZT and the shape dimensions of compliant parts have to be investigated in views of motion and strength of compliant mechanical amplifiers.

The PZT bonded to the driving compliant bridge induces the uniform deformation on it. For making the relationship between PZT deformation and mechanical

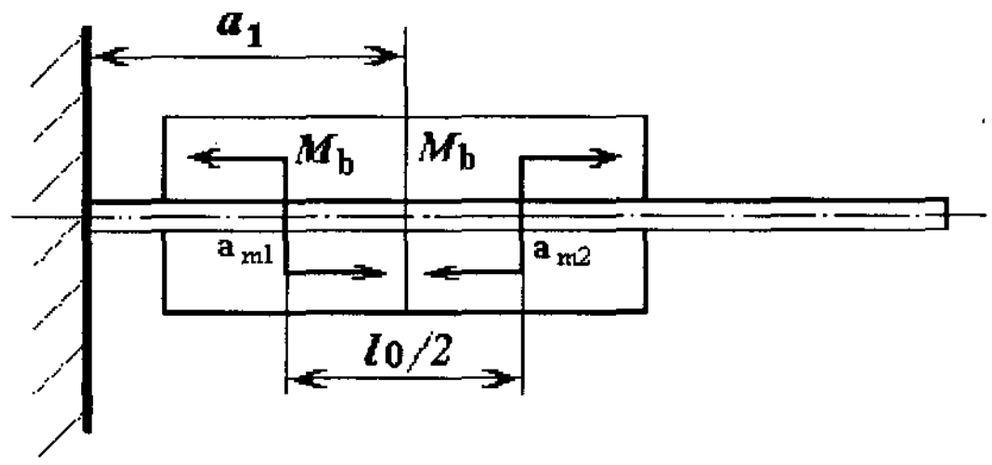

Fig. 4 Bending moment of compliant bridge under alternating PZT loading

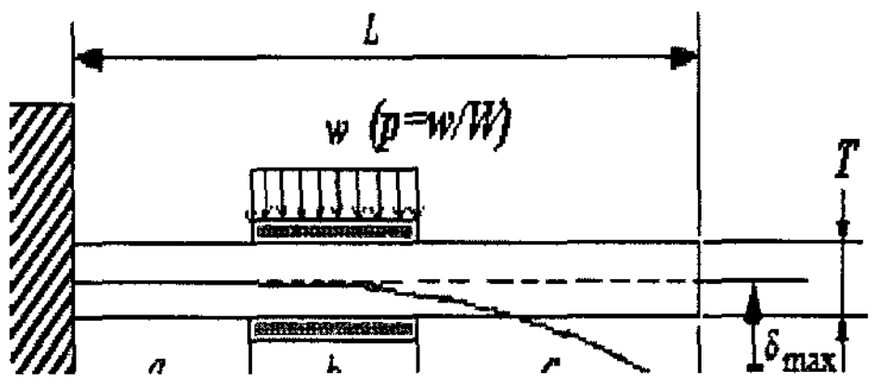

(a) Mechanical loading condition

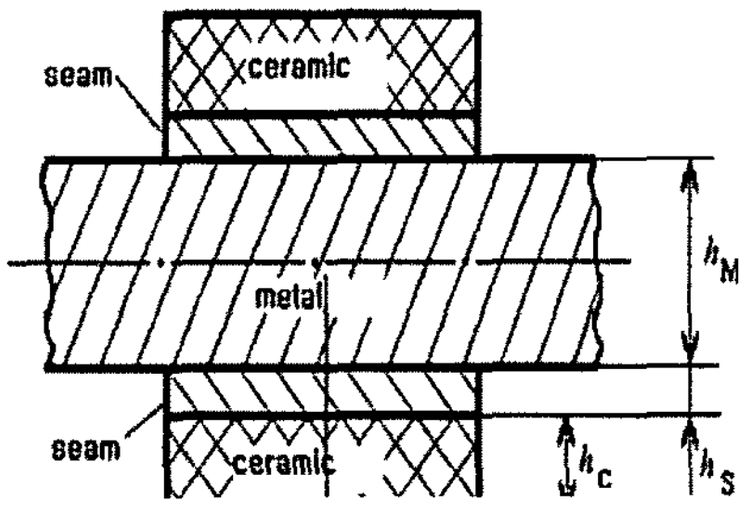

(b) PZT bonding configuration

Fig. 5 PZT loading configuration

loading condition, the PZT configuration shown in Fig. 5 is used.

PZT is attached to both sides of compliant bridge and the maximum bending deformations due to moment loading and uniformly distributed loading can be assumed to be the same.

$$\delta_{\max}(M_b) = \delta_{\max}(w) \tag{5}$$

$$\delta_{\max}(M_b) = \frac{l_c(l-a_1)}{EI}(2M_b) = 2\frac{b\left(b/2+c\right)}{EI}M_b \tag{6}$$

$$\delta_{\max}(w) = \frac{wb}{EI}\left[\frac{L^3}{6} - \left(a+\frac{b}{2}\right)\frac{L^2}{2} - \frac{\left(b/2+c\right)^3}{6} - \frac{b^2L}{24} - \frac{b^2}{8}\left(\frac{a}{3}+\frac{b}{2}\right)\right] \tag{7}$$

where, E is the Young's modulus of compliant bridge, $I = WT^3/12$, the bending moment, and M_b can be written by the force created by the piezo ceramic depending on its geometric dimensions, physical properties and the electrical voltage V supplied to the compliant bridge as shown in Fig. 5-b,

$$M_b = \frac{2EI}{T}\frac{\Delta L}{l_c} = F_c h_\Sigma = F_c(h_M + h_c + 2h_s) \tag{8}$$

$$F_c = \frac{q_c}{2d_{31}} = \frac{C_c V}{2d_{31}} = \frac{\varepsilon\varepsilon_0 S_c V}{2h_c d_{31}} \tag{9}$$

where, q_c is the charge on the piezoceramic plates, C_c is its capacitance, S_c is the area of the piezoceramic plates, h_c is the thickness of piezo element, h_s is the thickness of seam, h_M is the thickness of elastic metal (T), ε is the relative dielectric permeability of the piezoceramic, ε_0 is the dielectric constant, and d_{31} is the transverse piezo modulus.

Using eqs. (5)-(9), the uniformly distributed loading, w, can be written by

$$2\frac{b\left(b/2+c\right)}{EI}\cdot\frac{\varepsilon\varepsilon_0 S_c V}{2h_c d_{31}}\cdot(h_M + h_c + 2h_s) = \frac{wb}{EI}\left[\frac{L^3}{6} - \left(a+\frac{b}{2}\right)\frac{L^2}{2} - \frac{\left(b/2+c\right)^3}{6} - \frac{b^2L}{24} - \frac{b^2}{8}\left(\frac{a}{3}+\frac{b}{2}\right)\right] \tag{10}$$

The pressure due to PZT can be expressed by.

$$p = w/W = \frac{2b\left(b/2+c\right)\cdot\frac{\varepsilon\varepsilon_0 S_c V}{2h_c d_{31}}\cdot(h_M + h_c + 2h_s)}{Wb\left[\frac{L^3}{6} - \left(a+\frac{b}{2}\right)\frac{L^2}{2} - \frac{\left(b/2+c\right)^3}{6} - \frac{b^2L}{24} - \frac{b^2}{8}\left(\frac{a}{3}+\frac{b}{2}\right)\right]} \tag{11}$$

3. Design of Compliant Mechanical Amplifiers

In the compliant mechanisms, the displacements add up all elastic deformation and pseudo-rigid body motions of all sequent members covering the links of the mechanism. If only bending and axial effects are taken into account in the planar compliant mechanism the displacements at arbitrary node l are formulated by means of Castigliano's second theorem[11].

$$u_{lx} = \frac{\partial U}{\partial F_{lx}} = \sum_{i=l}^{n}\left(\int_0^{l_i}\frac{M_{bi}}{E_i I_i Z_i}\frac{\partial M_{bi}}{\partial F_{lx}}dx_i + \int_0^{l_i}\frac{N_i}{E_i A_i}\frac{\partial N_i}{\partial F_{lx}}dx_i\right)$$

$$u_{ly} = \frac{\partial U}{\partial F_{ly}} = \sum_{i=l}^{n}\left(\int_0^{l_i}\frac{M_{bi}}{E_i I_i Z_i}\frac{\partial M_{bi}}{\partial F_{ly}}dx_i + \int_0^{l_i}\frac{N_i}{E_i A_i}\frac{\partial N_i}{\partial F_{ly}}dx_i\right)$$

$$\theta_{lz} = \frac{\partial U}{\partial M_{lz}} = \sum_{i=l}^{n}\left(\int_0^{l_i}\frac{M_{bi}}{E_i I_i Z_i}\frac{\partial M_{bi}}{\partial M_{lz}}dx_i\right) \tag{12}$$

where, F_{lx}, F_{ly} and M_{lz} are the forces and moment at node l. U is the strain energy. From eq. (12), the displacements are the functions of compliances of various flexure hinges as follows.

$$u_{lx} = \sum_{i=l}^{n}\left(A_{ix}C_{i,x-F_x} + B_{ix}C_{i,y-F_y} + D_{ix}C_{i,y-M_z} + H_{ix}C_{i,\theta_z-M_z}\right)$$

$$u_{ly} = \sum_{i=l}^{n}\left(A_{iy}C_{i,x-F_x} + B_{iy}C_{i,y-F_y} + D_{iy}C_{i,y-M_z} + H_{iy}C_{i,\theta_z-M_z}\right)$$

$$\theta_{lz} = \sum_{i=l}^{n}\left(D_{i\theta_z}C_{i,y-M_z} + H_{i\theta_z}C_{i,\theta_z-M_z}\right) \tag{13}$$

where, A_i*, B_i*, D_i* and H_i* are the configuration coefficients.

Using eq. (13) in the complex compliant mechanism,

it is difficult to develop the general compliant mechanism geometric configuration and the various compliances of the flexure hinges that compose the mechanism. In this paper, the locations of rotational flexure hinges are defined on the base of the lever ratio called to geometric advantage factor. The compliant mechanism used in this system is 5.0 which is the ratio of output displacement to input displacement. For finding the geometric dimensions in the corner-filleted flexure hinges, the shape optimization technique is utilized.

In the micro-positioning mechanisms, the compliant bridge and flexure hinge has been commonly used. The infeasible design of compliant mechanism deteriorates the positioning accuracies. The amplification ratio is defined as the geometric advantage (GA).

$$MAX\,(GA)=\frac{\{\delta_o\}^T\{F_o\}}{\{\delta_i\}^T\{F_i\}}=\frac{\{\delta_o\}^T[K]\{\delta_o\}}{\{\delta_i\}^T[K]\{\delta_i\}},$$

$$\text{subject to } volume \le V_O \tag{14}$$

where, $[K]$ is the global stiffness matrix. In this paper, the compliant mechanical amplifier is made of aluminum, which has the mechanical properties shown in Table 1. The mechanical specifications of the compliant mechanical amplifier of 3-DOF parallel micromanipulator are shown in Table 2.

The shape optimization process is performed for the feasible compliant bridge and flexures hinge meeting the structural performances such as stiffness, strength and motion straightness. Generally, a typical optimization design problem of minimizing an objective function that is subject to a set of constraints can be written by

$$\begin{aligned} &Find \quad \rho \\ &\min \quad \psi(\mu,\rho) \\ &subject\ to \quad G_k(\mu,\rho), k=1,\ldots,m \end{aligned} \tag{15}$$

where, ρ is the geometric dimension of corner-filleted flexure hinges and μ represent the structural variables such as stress, stiffness and motions. The optimization process can be described as an iterative search process that uses the following steps:

① Define the initial stress state of an initial design $\rho^{i=0}$ for the PZT loading environments; $[K_0]\{u_0\}=\{F_0\}$

② The design variables are predicted for satisfying stress and stiffness under the loading condition. $\rho^{i+1}=\rho^i+\delta\rho^{i+1}$.

③ Compare the element stress in the given structure with the allowable stress.

④ If the requirements are not met, perform the optimization routine in order to set of $\delta\rho$.

⑤ Correct $\delta\rho^{i+1}$ based on the stress ratio design with $\beta=0.9$,

$$\left(\delta\rho^{i+1}\right)_{new}=\left(\delta\rho^{i+1}\right)_{old}\left(\frac{\eta_{element}}{\eta_{allowable}}\right)^{\beta} \tag{16}$$

where,

$$\left(\delta\rho^{i+1}\right)_{old}=S^i\cdot\alpha=\left(-\nabla\psi^i+\frac{\left|\nabla\psi^i\right|^2}{\left|\nabla\psi^{i-1}\right|^2}S^{i-1}\right)\cdot\left(\frac{\delta\psi^i}{\left(\nabla\psi^i\right)^T S^i}\right),$$

$\eta_{allowable}$ is the average stress and $\eta_{element}$ is the stress of each element.

⑥ If the requirements are satisfied, perform the discrete design for the design variables with consideration of manufacturability tolerance μ. Otherwise, go to step 2.

Fig. 6 shows the conceptual compliant mechanical amplifier through the shape optimization design and structural performances. Table 3 shows the vertical displacement under PZT loading. The loading condition is the

Table 1 Material properties

	E(GPa)	Poisson's ratio, ν	Density, (ton/m^3) ρ	(MPa) σ_y
value	69	0.29	2.76	200

Table 2 Mechanical specifications

	Vertical motion of output zone (μm)	Vertical motion of input zone (μm)	Upper limit of Effective stress (MPa)
value	100	15	67

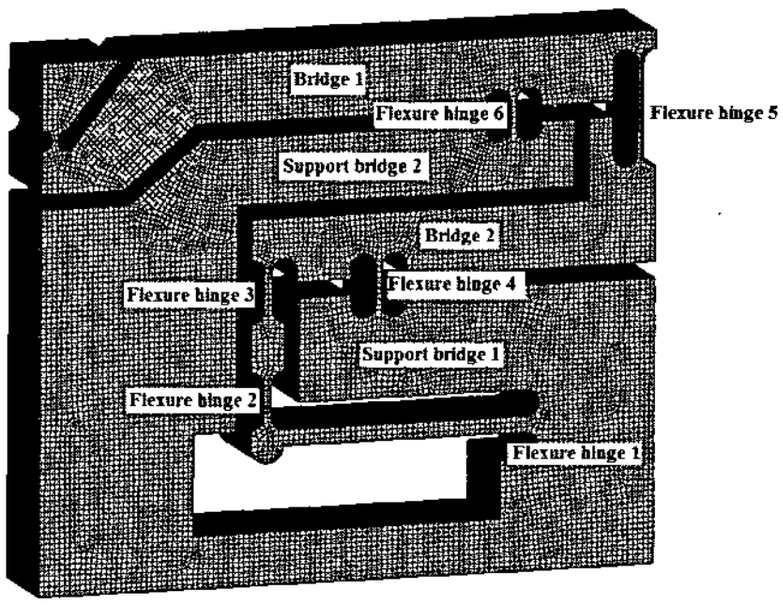

(a) Conceptual simulation model

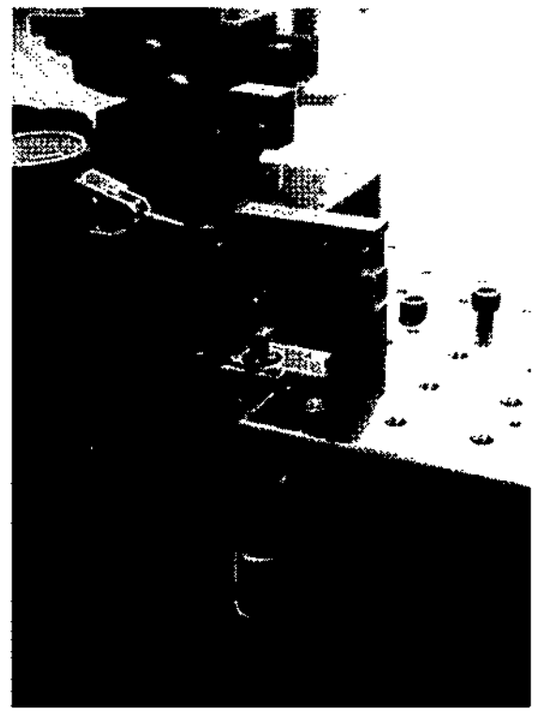

(b) Manufactured model

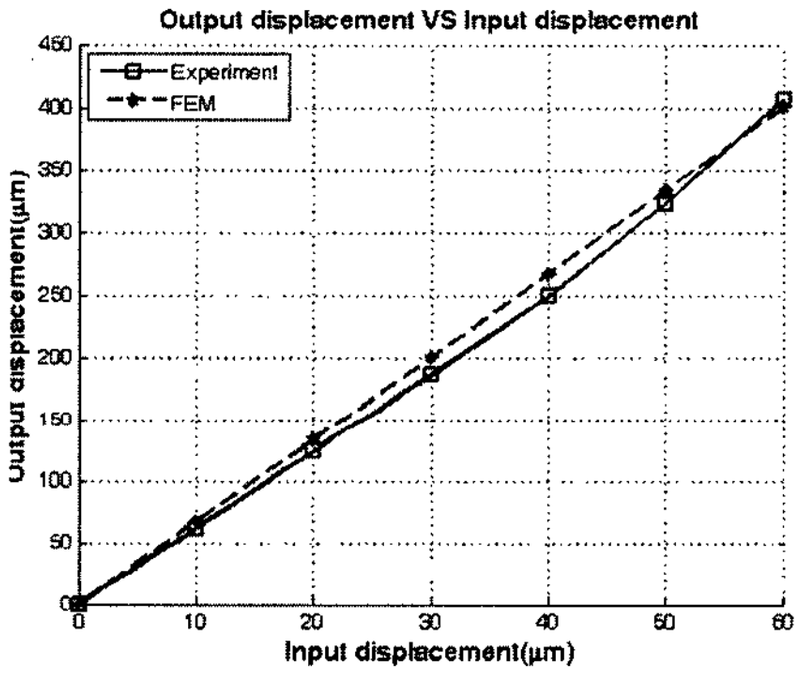

(c) Simulation and experiment results under PZT loading

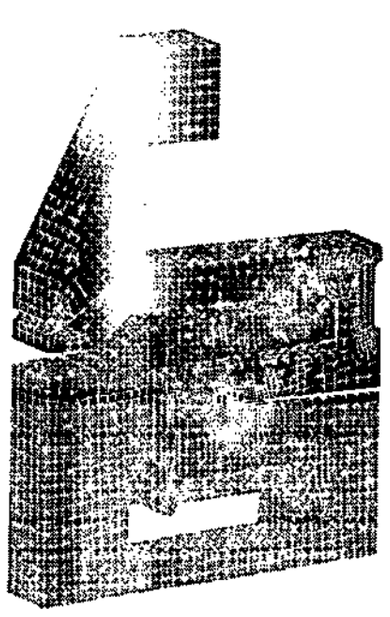

(d) Displacement contour (unit: mm)

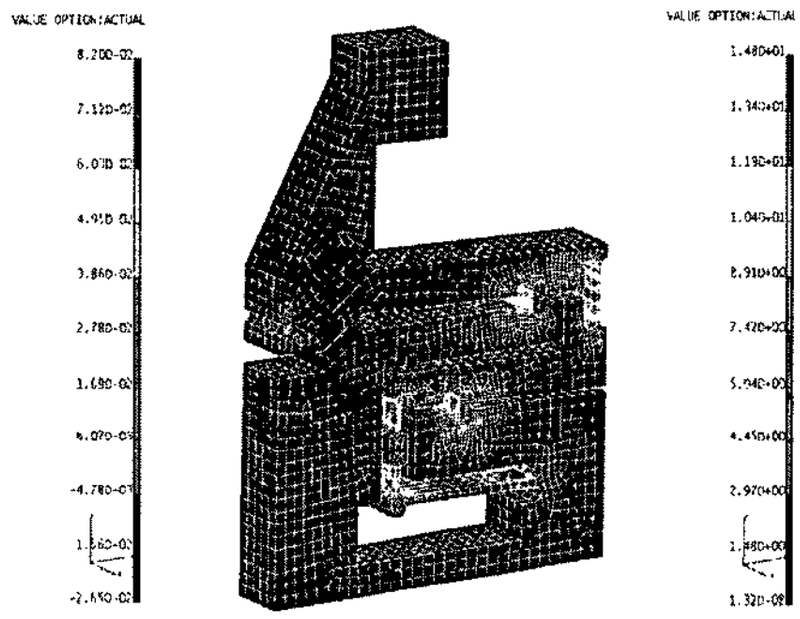

(e) Stress contour (unit: MPa)

Fig. 6 Schematic compliant mechanical amplifier

Table 3 Output displacement versus input displacement under PZT loading

PZT loading Disp. (mm)	Output Disp. (mm)
0	0
2.57E-03	0.017553865
5.14E-03	0.03510773
7.71E-03	0.052661602
1.03E-02	0.070215474
1.29E-02	0.087769325
1.54E-02	0.105323176
1.80E-02	0.122877096
2.06E-02	0.140430947
2.31E-02	0.157984798
2.57E-02	0.17553865

vertical forces equivalent to the vertical motion of PZT stack. The GA is 6.67 and the maximum stress is 18.4MPa.

4. Simulation

Under the maximum operation (90 μm) of compliant amplifier, the structural performance of 3 DOF parallel micro-manipulator is investigated. Fig. 7 shows the displacement contour and Fig. 8 shows the stress contour, under the maximum operation. The maximum vertical motion is 443 μm. The deviations of driving leg and support are 17% and 1.5% relative to the vertical motion, respectively. As the fundamental dynamic characteristics, Fig. 9 shows the normal mode. The response time is 0.014 sec. And this simulated micro-manipulator is newly presented as

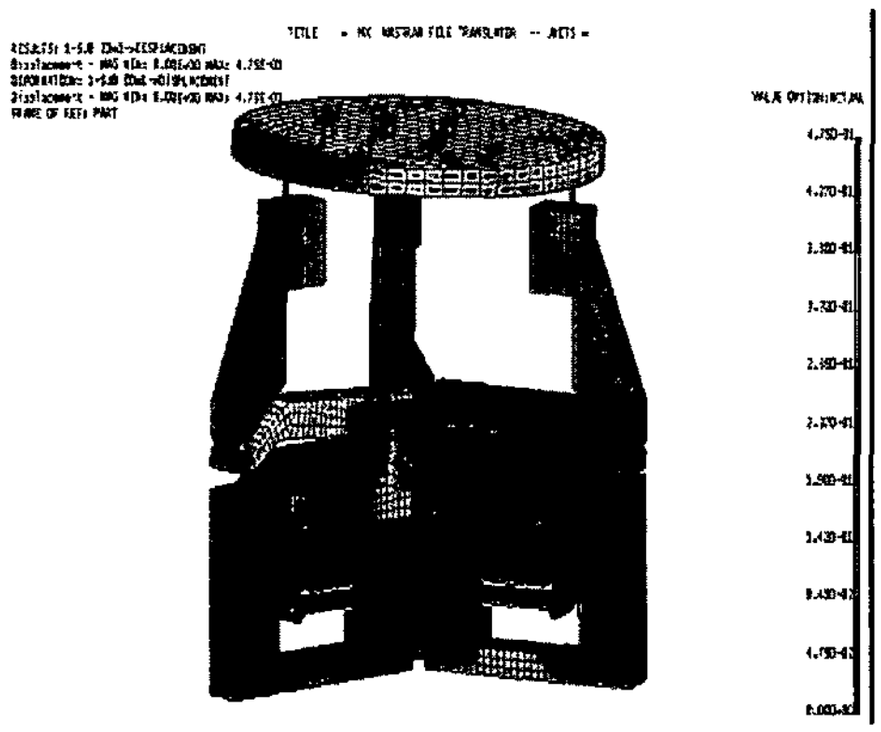

(a) Overall deformation contour under PZT loading

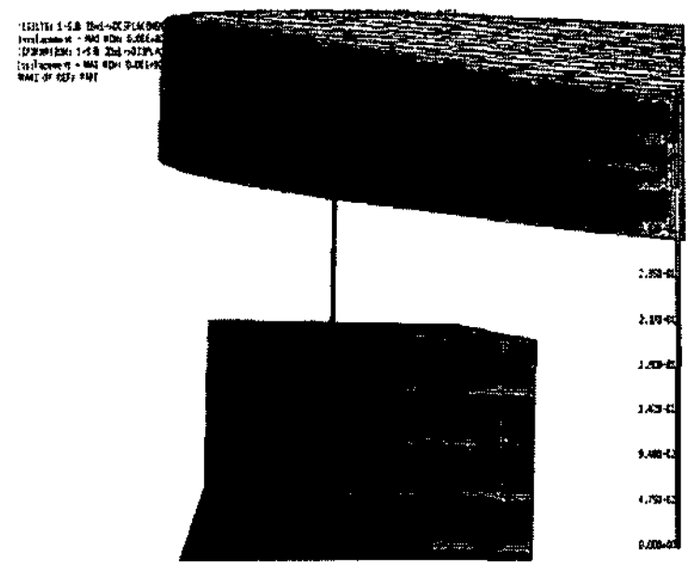

(b) Tip contour of Support leg 1

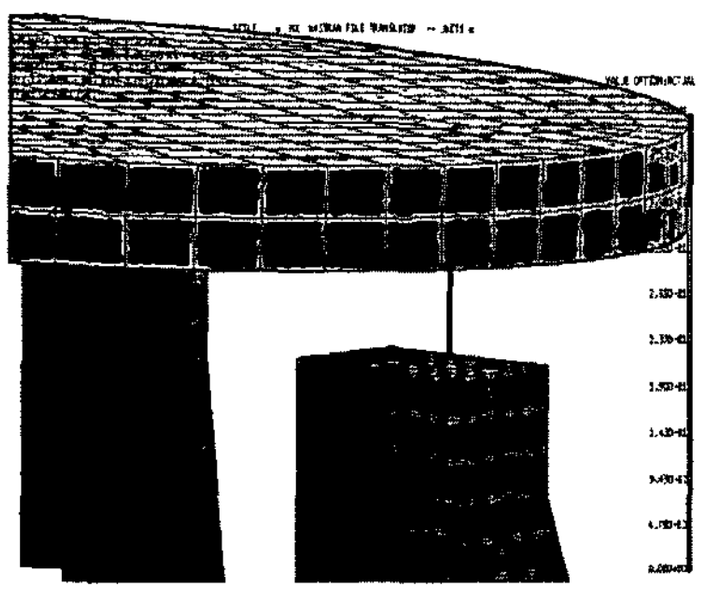

(c) Tip contour of Support leg 2

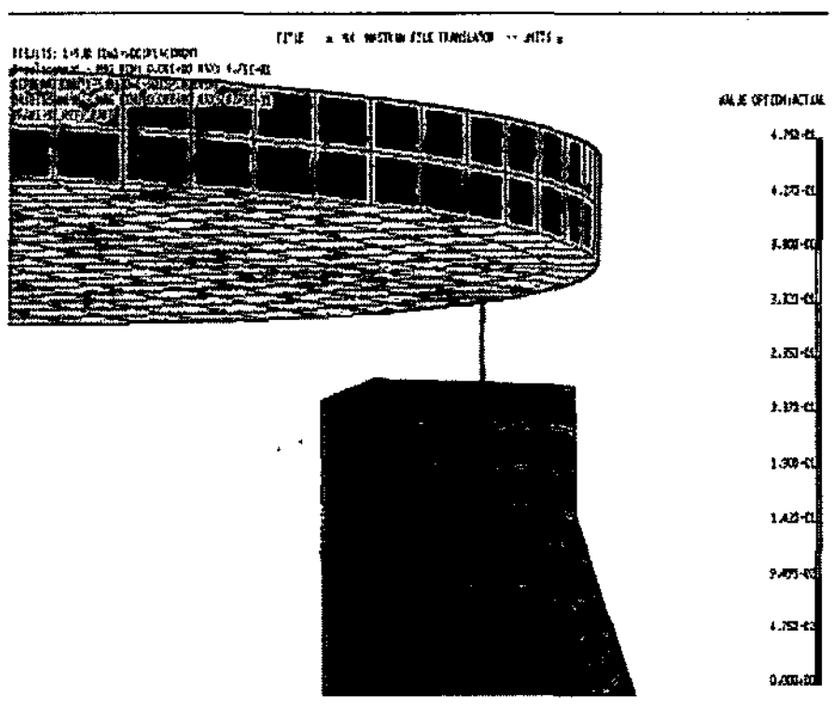

(d) Tip contour of Support leg 3

Fig. 7 Deformation contour of parallel micro-manipulator

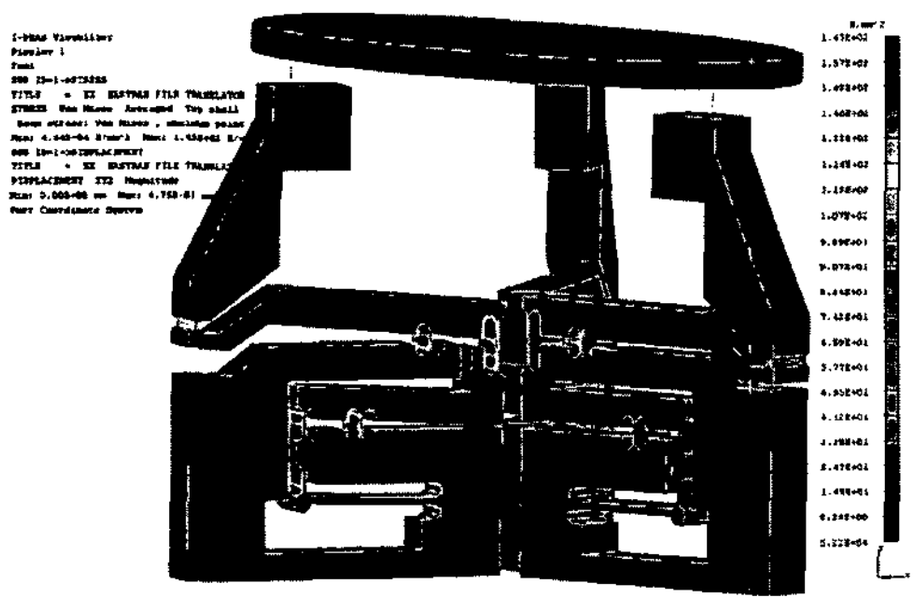

Fig. 8 Stress contour of parallel micro-manipulator

the iterative design method to secure the feasible structural performance and micro-positioning mechanism of a micro flexural hinge structure with geometric-material. Based on the kinematic simulation and experiment of 3-DOF parallel micromanipulator, the workspaces for first model, shape optimized model and manufactured model are calculated and compared(Fig. 8). In case that the workspace of first model is 1, the workspaces for shape optimized model and manufactured model are about 250 and 185 times. Therefore manufacture 3-DOF parallel manipulator with compliant mechanical amplifier has wider workspace than the first model without compliant mechanical amplifier as shown in Fig. 10.

5. Conclusion

This paper presents the iterative design method to secure the feasible structural performance and micro-positioning

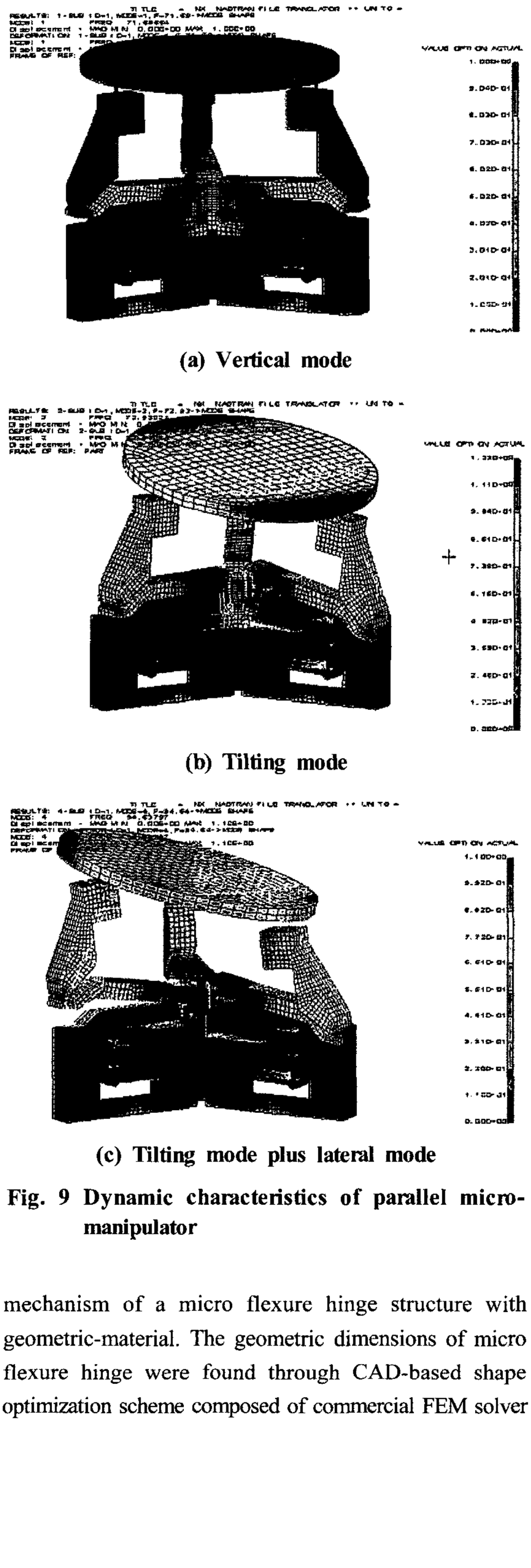

(a) Vertical mode

(b) Tilting mode

(c) Tilting mode plus lateral mode

Fig. 9 Dynamic characteristics of parallel micro-manipulator

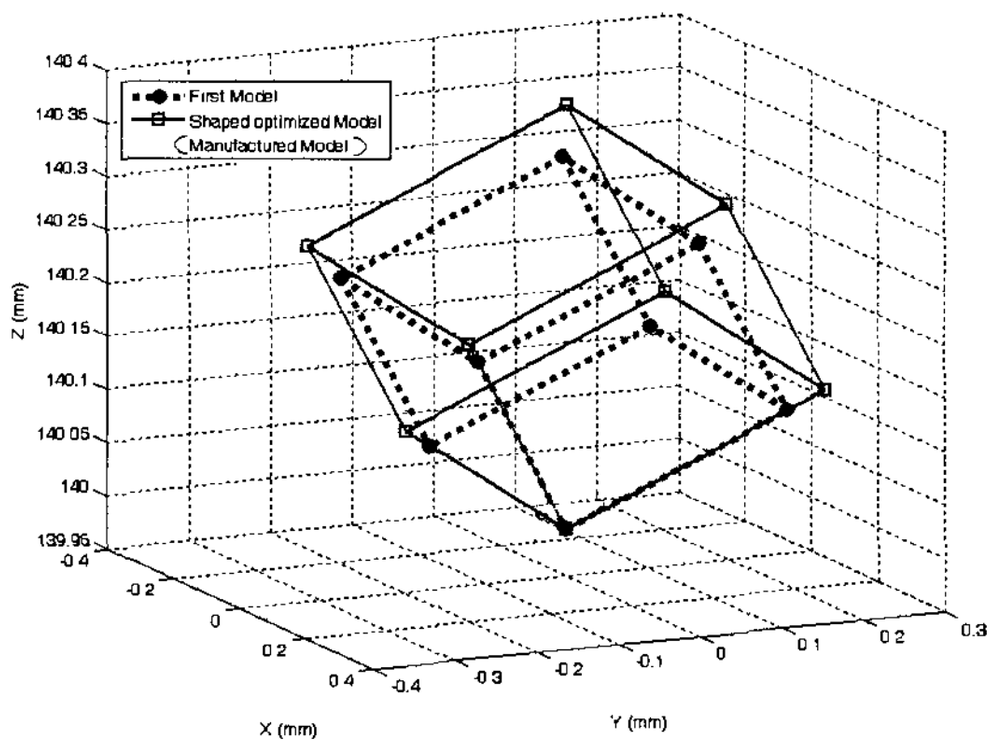

Fig. 10 Comparison of operation workspaces

mechanism of a micro flexure hinge structure with geometric-material. The geometric dimensions of micro flexure hinge were found through CAD-based shape optimization scheme composed of commercial FEM solver and sequential linear programming in the NX-IDEAS. For the correction of design variables, the ratio of element stress to average stress is used. The effectiveness of this design methodology is shown through simulation. This work can be emphasized as follows:

(1) The precise design modeling of a flexure hinge mechanism is significant to ensure the positioning accuracy of parallel micro-mechanism with flexure hinges.

(2) The basic dimensions are based on the topology optimization design of parallel micro-mechanism with flexure hinges.

(3) Using the ratio of element stress to average stress, the design variables are corrected.

References

(1) Alfred, E. T. and Delbert, T., 1990, "Using CAD/CAM in the design of a robotic micromanipulator," *Computer-Aided-Engineering Journal*, Vol. 7, pp. 43~48.

(2) Ryu, J. W., Lee, S. Q., Gweon, D. G., and Moon, K. S., 1999, "Inverse kinematic modeling of a coupled flexure hinge mechanism," *Mechatronics*, Vol. 9, pp. 657~674.

(3) Gao, P., Swei, S. M., and Yuan, Z., 1999, "A new piezo-driven precision micropositioning stage utilizing

flexure hinges," *Nanotechnology*, Vol. 10, pp. 394~398.
(4) Singiresu, S. R., 1996, *Engineering optimization-theory and practice*, Third edition, John Wiley & Sons. New York, pp. 84~96.
(5) Bendsoe, M. P. and Kikuchi, N., 1988, "Generating optimal topologies for structural design using a homogenization method," *Computer Methods in Applied Mechanics & Engineering*, Vol. 71, pp. 197~224.
(6) Bendsoe, M. P., 1989, "Optimal shape design as a material distribution problem," *Structural Optimization*, Vol. 1, pp. 193~202.
(7) Jog, C. S. and Haber, R. B., 1996, "Stability of finite element models for distributed parameter optimization and topology design," *Computer Methods in Applied Mechanics & Engineering*, Vol. 130, pp. 203~226.
(8) Choi, H. S., Lee, D. C., Kim, S. S., and Han, C. S., 2005, "The development of a microgripper with a perturbation-based configuration design method," *Journal of Micromechanics and Microengineering*, Vol. 15, pp. 1327~1333.
(9) Tak, T. Y., Lee, D. C., and Han, C. S., 2006, "Mechanical Analysis and Design of 3 Degree Freedom Parallel Micromanipulator," *Proceedings of the Korean Society of Machine Tool Engineers*, Vol. 1, pp. 129~133.
(10) Wempner, G. A., 1971, "Discrete approximations related to nonlinear theories of solids," *International Journal of Solids and Structures*, Vol. 7, pp. 1581~1599.
(11) Robert, D. C., David, S. M., and Michael, E. P., 1989, *Concepts and applications of finite element analysis*, Third edition, John Wiley & Sons. New York, pp. 98~125.
(12) Nicolae, L., 2003, *Compliant mechanisms; Design of flexure hinges*, CRC Press LLC. US.
(13) Cho, J. R., Yang, S. C., and Jung, Y. G., 2006, "A Study on the Improvement of Performance for High Speed Cutting Tool using Magnetic Fluid Polishing Technique," *Transactions of the Korean Society of Machine Tool Engineers*, Vol. 15, No. 1, pp. 32~38.
(14) Kim, H. G., Kim, Y. S., Yang, S. M., and Nah, S. C., 2005, "A Study on Unit Cell Design for the Performance Enhancement in PEMFC System," *Transactions of the Korean Society of Machine Tool Engineers*, Vol. 14, No. 4, pp. 104~109.